

Wind loads on solar panels mounted parallel to pitched roofs, and acting on the underlying roof

C.J. Leitch^{*1}, J.D. Ginger¹ and J.D. Holmes²

¹*Cyclone Testing Station, School of Engineering and Physical Sciences, James Cook University,
Townsville, Queensland, Australia*

²*James Cook University, Townsville and JDH Consulting, Mentone, Victoria, Australia*

(Received December 5, 2014, Revised December 4, 2015, Accepted December 18, 2015)

Abstract. This paper describes an investigation of the net wind loads on solar panels and wind loads on the underlying roof surface for panels mounted parallel to pitched roofs of domestic buildings. Typical solar panel array configurations were studied in a wind tunnel and the aerodynamic shape factors on the panels were put in a form appropriate for the Australian/New Zealand Wind Actions Standard AS/NZS 1170.2:2011. The results can also be used to obtain more refined design data on individual panels within an array. They also suggest values for the aerodynamic shape factors on the roof surface under the panels, based on a gust wind speed at roof height, of ± 0.5 for wind blowing parallel to the ridge, and ± 0.6 for wind blowing perpendicular to the ridge. The net loads on solar arrays in the middle portion of the roof are larger than those on the same portion of the roof without any solar panels, thus resulting in increased loads on the underlying roof structure.

Keywords: wind load; solar panel; code; standard; low-rise building; roof

1. Introduction

There is now wide-spread use of photovoltaic solar panel systems mounted on roofs of houses (i.e., low rise buildings) for power generation. Commonly in Australia and other countries, an array of panels is attached to support rails and parallel to the sloping surface of the roof, with a gap, between the panel and the roof below, of 100 to 200 mm. The wind loads on these panel arrays must be quantified so that the structural supports of both the panel mounting system and the roof can be assessed. Although some research has been carried out recently, there are limited wind loading data (in codes and standards) for the design of these systems.

This paper describes a wind tunnel study that determined wind pressures on solar panel arrays, mounted parallel to the roof of typical, domestic buildings, and the roof surface below these panels. The overall results from that study were described by Ginger *et al.* (2011), and form the basis of the revised design data given in the amendment to the Australian/ New Zealand Standard on Wind Actions, AS/NZS 1170.2 (Standards Australia 2011).

Several previous studies have quantified wind loads on roof-mounted solar panel arrays by

*Corresponding author, Researcher, E-mail: campbell.leitch@jcu.edu.au

means of full scale experiments on small solar panel arrays, and wind tunnel studies using scaled models. Wood *et al.* (2001) carried out a wind-tunnel model study at 1/100 scale on a low-rise, flat-roofed, rectangular building of plan dimensions 41 m × 27 m in an open country (Terrain Category 2) boundary layer profile, as defined in AS/NZS 1170.2 (Standards Australia 2011). Eight model panels, each 4.1 m × 2.7 m × 0.3 m in full-scale, were placed above and parallel to the flat roof, with three different clear heights of 6, 10 and 14 mm (in model scale) between the top of the roof and underside of the panels and three different lateral gaps of 4, 6 and 8 mm between the panels. Fluctuating pressures were measured over one quarter of the roof, at each of ten locations using three pressure taps, one each on the panel topside, panel underside and top of roof. The peak net uplift pressure coefficients on the panels were all significantly lower in magnitude than those for the corresponding uplift for the roof, with no panels attached, but the peak net down-thrust values were all greater. However, the smallest gap between panel and roof was 600 mm (in full-scale), and hence may not satisfactorily simulate residential installations where this gap is typically only 100 to 200 mm. This is a difficulty faced when modelling at a small scale and ensuring an adequate simulation for wind flow through narrow gaps with sufficiently high Reynolds Number, as advised by Kopp and Banks (2013) and adopted by Kopp (2014), who used a 1/30 scale model.

Stenabaugh *et al.* (2011) undertook a wind tunnel study using 1:20 scale models of typical two-storey residential buildings, to investigate wind loads on solar panels. They used two models, the first with full-scale plan dimensions of 10 m × 15 m and a roof pitch of 45°, the second model used plan dimensions of 12.25 m × 15 m, and a roof pitch of 30°, to maintain a constant roof surface area. Both models were equipped with a 4 × 7 solar panel array, with an overall full-scale size of nominally 3.5 m × 5.8 m, that was tested in six positions on the roof, and with two air gaps of either 40 mm or 80 mm (in equivalent full-scale) between the top of the roof and the underside of the panels. The solar PV panels were constructed with an overall thickness of 10 mm to allow pressure tap tubes to be located within the panel thickness. The blockage typically caused by the rail-mounting system was modelled by allowing these tubes to exit the solar panel array in lines on both longitudinal sides of the panel array. A total of seventy-seven taps were placed on the upper and lower surfaces of the PV array and two hundred and twenty-four taps placed on the roof surface.

Stenabaugh *et al.* (2011) used simulated boundary layer wind flow over open-country terrain, and pressure coefficients were obtained for the roof surface, and the bottom and top surfaces of the panels. They found that the mean pressure coefficients for the roof surfaces under the panels were virtually identical to those on the bottom surface of the panels above. They also found that the addition of a solar array has minimal impact on overall structural wind loads on the roof. Area-averaged net pressure coefficients were calculated for all taps within a nominated area ranging from just one panel (about 0.7 m²) to all 28 panels (about 20 m²). These net pressure coefficient values reduced in magnitude as the tributary area increased up to about 10 m² and then were approximately constant up to about 20 m², the upper limit of area of the panel array that was investigated. They concluded that the wind loads were higher with the array located at the edge of the building and also increased with the higher roof slope. However, varying the spacing between the array and the roof did not have a significant effect on the wind uplift loads on the solar panels. More recent work by these authors has included the effects of varying the lateral gap spacing between individual modules.

Stathopoulos *et al.* (2014) conducted a wind tunnel study using 1:200 scale models of two flat roofed buildings of full-scale plan size of 30.6 m × 19.6 m, roof heights of 7 m and 16 m, with the

tests performed using the most critical open terrain exposure. Solar panel arrays with full-scale dimensions of 25.8 m (length) \times 5.6 m (width) were mounted on the flat roofs of the buildings with four different inclinations of 20°, 30°, 40° and 45° to the horizontal. For each angle of inclination, the panels were mounted at two locations on the roof, with the lowest panel edge being either 4.4 m or 10.4 m from the “front” (30.6 m long side) of the building. The inclination mechanism caused a small gap between the lower edge of the inclined panel and the surface of the flat roof, which is representative of normal installation practice. Eighteen pressure taps were fitted to both the top and bottom surfaces of the panels (thirty-six in total), so allowing upper, lower and net pressure coefficients to be determined. The buildings (with panel arrays attached) were symmetric and the tested wind directions were varied in 15° increments.

Stathopoulos *et al.* (2014) found that the effect of wind direction is significant with the largest magnitude pressure coefficients occurring within a 75° range of wind directions (105° - 180°), but the effect of panel inclination is significant only for critical wind directions. They also found that the effect of building height and exact panel location were not very significant, but panels near the roof edges experienced the greatest net force coefficients. However, as this study used inclined panels mounted on a flat roof their results cannot be used for deriving loads on panels mounted parallel to the roof surface.

Maffei *et al.* (2014) and Kopp (2014) obtained design wind load data on a range of solar panel configurations for a range of tilt angles on a nearly flat roof. Wind-tunnel tests were carried out at a length scale of 1/30 in approach boundary layer flow for panels tilted at 2°, 5°, 10°, 20°, and 30°. Data was provided in a form that can be incorporated in ASCE-7-10 (American Society of Civil Engineers 2010). Again, the configurations tested in these studies were not representative of the typical set-up applied to domestic houses and considered in this paper.

Schellenberg *et al.* (2013) carried out dynamic analysis on a solar panel structural system with panels inclined on a flat roof. They showed that the wind loads can be satisfactorily derived using static analysis methods such as those prescribed in codes and standards, i.e., ASCE-710 (American Society of Civil Engineers, 2010).

Cao *et al.* (2013) determined wind loads on flat panel “green roofing” modules that are becoming widely used on flat roofs. They also studied the influence of parapets on the loads. Modules located near corners were found to experience the highest loads and these loads exceeded values given in ASCE-7-10 (American Society of Civil Engineers, 2010).

A wind tunnel model study was carried out on solar arrays mounted on single story domestic gable-end roof houses with roof slopes of 7.5°, 15° and 22.5° and documented in a comprehensive report produced by Ginger *et al.* (2011). This paper presents the results for the most common cases of a solar panel array mounted adjacent to the gable end, and the middle third of the roof for a 22.5° roof slope house. The paper also derives the wind loads on individual panels along the array and the roof surfaces below the panels. Further analysis was carried out to derive design wind loading data that is required for the design of the panels, and the structural system, that can be used to produce (or update) data available in the Australian/New Zealand Standard, AS/NZS 1170.2:2011.

2. Wind tunnel investigation

The report, by Ginger *et al.* (2011) provided a detailed account of the wind tunnel study. The pressure coefficients obtained can be combined with the design wind speed as defined in

AS/NZS 1170.2:2011 to produce the net design pressure on the solar panels and the external design pressure on the roof of the building. These data can also be used with other codes and standards, by applying conversion factors given by Holmes and Ginger (2012) with design wind speeds that have other gust durations, such as those specified in ASCE7-10 (American Society of Civil Engineers, 2010).

2.1 Building and panel details

The wind tunnel tests were carried out on a 10 m x 21 m x 2.7 m representative house shown in Fig. 1 at a length scale (L_r) of 1/20 in the 2.1 m high x 2.5 m wide x 22 m long boundary layer wind tunnel at James Cook University. Three gable roof models with pitch slopes (α) of 7.5°, 15° and 22.5° were constructed to represent the range of houses. A total of thirty-two pressure taps were installed over one quarter of the roof surface of the models, as shown in Fig. 1 to measure external roof surface pressures. Also shown in this Figure are the four orthogonal wind directions ($\theta = 0^\circ, 90^\circ, 180^\circ, 270^\circ$) and a solar array fitted to the building.

The model buildings, both with and without solar arrays, were tested in the wind tunnel with an approach atmospheric boundary layer to simulate a suburban approach terrain using an array of blocks on the floor of the upstream fetch of the wind tunnel. The mean velocity and turbulence intensity profiles of the approach flow are shown in Figs. 2(a) and 2(b) respectively. The turbulence intensity at mid roof height is about 0.23. The spectral density indicated that the turbulence length scale was about 1/3 of that suggested in AS/NZS11702:2011 for a height of 3 metres, but this limitation was similar in other studies carried out for determining the loads on the solar panels and should not adversely affect the outcomes, (Australasian Wind Engineering Society, 2001).

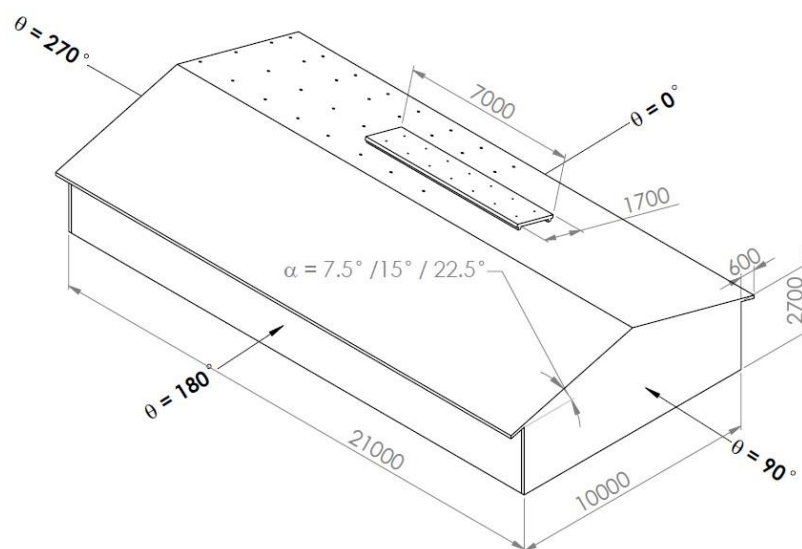


Fig. 1 10 m x 21 m x 2.7 m gable end house showing pressure tap locations. (1.7 m x 7.0 m solar panel array shown fitted to Position B)

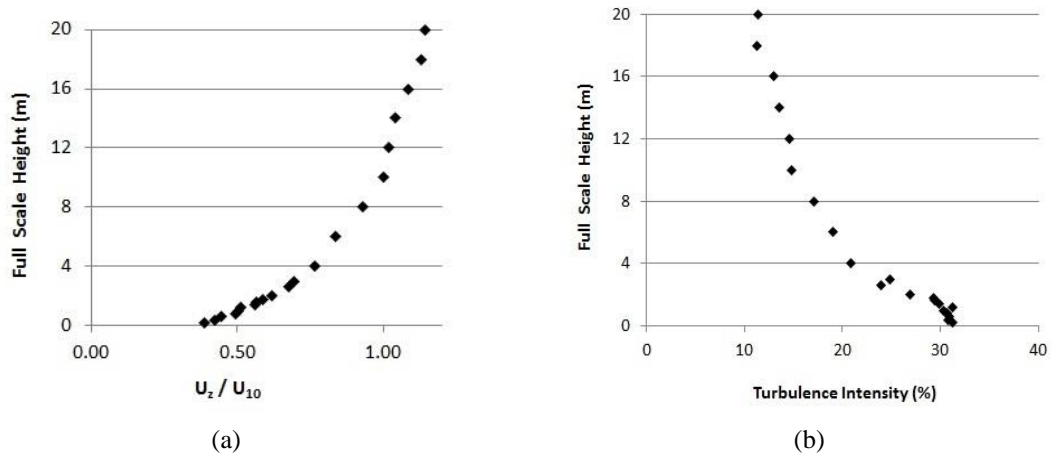


Fig. 2 (a) Mean velocity profile and (b) Turbulence intensity profile

An array consisting of seven panels, each with full-scale dimensions of $1.7 \text{ m} \times 1.0 \text{ m}$ was selected to model a representative solar panel system. The $85 \text{ mm} \times 350 \text{ mm}$ model scale solar panel array was constructed with a thickness of 6 mm so that small holes could be drilled within the thickness of the panels to form internal tubes for pressure tapping points on both the top and bottom surfaces. This also allowed measurement of net pressures across the panel. The 6 mm thickness (that equates to 120 mm in full scale) is thicker than a typical solar panel. However, the 6 mm thickness is an optimal arrangement to enable the inclusion of taps and tube and enable an open space under the panels. The increased thickness does not adversely influence the pressures measured at the mid panel locations. Fourteen pressure taps were installed to both the top and bottom panel surfaces of the 1×7 array aligned with each other (i.e., twenty-eight pressure taps in total), as shown in Fig. 3. These taps were used to obtain both top surface and bottom surface pressures on the panels, as well as net (i.e., (top-bottom)) pressures on each $1.7 \text{ m} \times 1.0 \text{ m}$ module. Fig. 3 also shows the layout of the support rails, spaced with an internal clear separation of 1300 mm and of sufficient height to provide either 100 mm or 200 mm (in full scale) clearance between the roof surface and the underside of the panels. The pressure taps from the model solar array were connected with tubes to pressure transducers through the two model rails that then ran inside the house model, so that there were no “loose tubes” in the gap between the panels and the top of the roof. This set-up satisfactorily represents typical full-scale panels and the flow over the roof surface as well as the gap between the roof surface and panels.

A configuration of the panels (one panel deep by seven panels long, 1×7) forming an array of $1.7 \text{ m} \times 7.0 \text{ m}$ was tested in six positions on the roof, identified as A, B, C, D, E and F. The results for all the configurations are reported by Ginger *et al.* (2011).

This paper focuses on results for the panel located at Positions B and D, as shown in Fig. 4.

Fig. 5 is a photograph that shows a house model with a 22.5° roof pitch and a solar panel array attached at Position D.

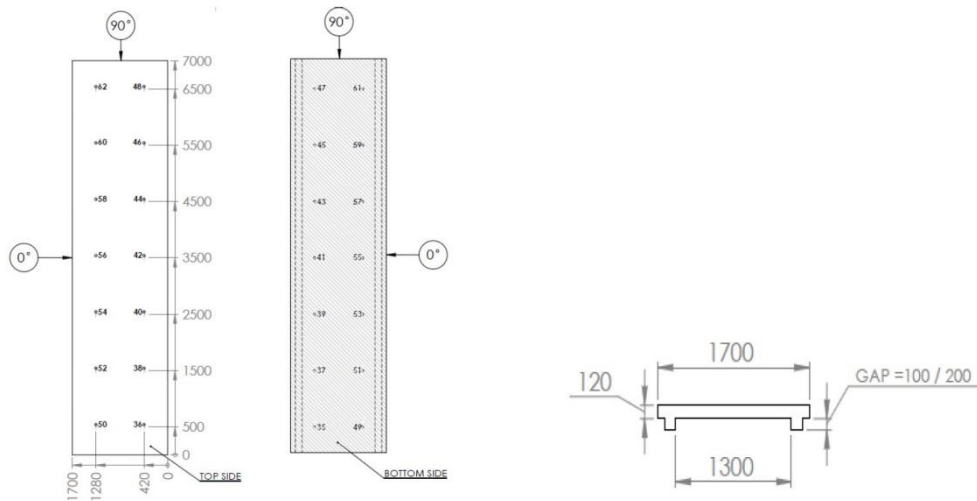


Fig. 3 1 × 7 module array and support system showing pressure tap locations on top and bottom surfaces. (All dimensions in mm)

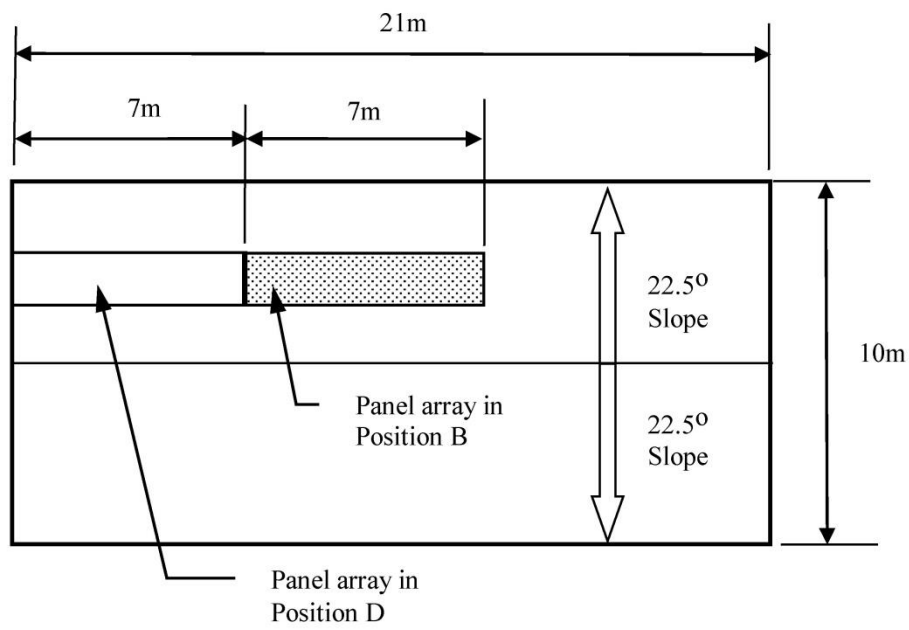


Fig. 4 Plan view of gable end house showing panel locations Position B and Position D



Fig. 5 Close-up view of the 22.5° roof pitch house model with a 1×7 solar panel array located at Position D in wind tunnel

2.2 Pressure coefficients and aerodynamic shape factors

External pressures were measured on the roof of the buildings for twenty-four approach wind directions $\theta = 0^\circ$ to 345° in steps of 15° (using the wind direction orientations shown in Fig. 1), for the building without solar panels, called the “baseline” building. Tests were repeated with solar panel arrays at each of the nominated locations, and the external pressures on the roof surface and the top and bottom surfaces of the solar panels were measured. The fluctuating pressures, $p(t)$ were sampled at 1250 Hz for 30 seconds and presented as pressure coefficients, $C_p(t) = p(t) / \frac{1}{2} \rho \bar{V}_h^2$. Here, $\frac{1}{2} \rho \bar{V}_h^2$ is the mean dynamic pressure at mid roof height h . These pressure coefficients were analysed statistically to calculate mean ($C_{\bar{p}}$), maximum ($C_{\hat{p}}$) and minimum ($C_{\check{p}}$) pressure coefficients in a single run

$$C_{\bar{p}} = \frac{\bar{p}}{\frac{1}{2} \rho \bar{V}_h^2}, \quad C_{\hat{p}} = \frac{\hat{p}}{\frac{1}{2} \rho \bar{V}_h^2}, \quad C_{\check{p}} = \frac{\check{p}}{\frac{1}{2} \rho \bar{V}_h^2} \quad (1)$$

Three runs were conducted for each approach wind direction to obtain repeated sets of pressure coefficients. The mean and peak (i.e., maximum and minimum) pressure coefficients presented in the study are the averages from the repeat runs. Area-averaged pressure coefficients on both the top and bottom of each $1.7 \text{ m} \times 1.0 \text{ m}$ panels were obtained by combining the simultaneous pressures on all taps for either the top or the bottom of each panel. The net (i.e., (top-bottom)) pressure coefficients, $C_{p,n}$ across the solar panels were also derived.

Design pressures can be obtained from the wind tunnel tests using Eq. (2), where ρ is the density of air, \bar{V}_h is the equivalent 10-minute mean wind speed at mid-roof height and C_{peak} is the maximum or minimum pressure coefficient.

$$p_{design} = 0.5\rho\bar{V}_h^2 C_{peak} \quad (2)$$

The peak wind loads for the design of structures and cladding using AS/NZS 1170.2:2011, and similar codes and standards based on a gust wind speed, are calculated from pressures derived from nominal shape factors or pressure coefficients, provided in the standard. The external design pressures are calculated from Eq. (3).

$$p_{design} = 0.5\rho V_h^2 C_{fig} \quad (3)$$

In Eq. (3), C_{fig} is the aerodynamic shape factor and V_h is the peak design gust wind speed (short duration, approximately 0.2 seconds) at mid-roof height.

These design external (or net) pressures derived from Eq. (3) for AS/NZS 1170.2:2011 can be equated to the values obtained by using Eq. (2) from the wind tunnel tests. Equating the design pressure from both Eqs. (2) and (3), results in Eq. (4).

$$p_{design} = 0.5\rho\bar{V}_h^2 C_{peak} = 0.5\rho V_h^2 C_{fig} \quad (4)$$

This equation can be simplified to relate the aerodynamic shape factor C_{fig} from the wind loading standard to the peak pressure coefficients C_{peak} from the wind tunnel data by Eq. (5).

$$C_{fig} = \left(\bar{V}_h^2 / V_h^2\right) C_{peak} \quad (5)$$

Note that in AS/NZS 1170.2:2011, the aerodynamic shape factor is calculated using the equation $C_{fig} = C_{p,e} (K_a K_c K_l K_p)$, where the quasi-static external pressure coefficient, $C_{p,e}$ is obtained from Section 5 of AS/NZS 1170.2:2011, and K_a , K_c , K_l and K_p are factors for area-averaging, load combination, local-pressure effects, and cladding permeability. However, this paper is utilizing the results from a wind tunnel study, incorporating all the effects described by the 'K' factors, and so the aerodynamic shape factor can be calculated directly using Eq. (5).

The 10-minute mean wind speed values can be estimated from Eq. (6).

$$\bar{V}_h = V_h / (1 + g_u I_u) \quad (6)$$

I_u is the turbulence intensity, which was measured in the wind tunnel as a function of height and g_u is a peak factor. Holmes *et al.* (2014) showed that a value of 3.4 for the peak factor is appropriate to relate the 0.2 second moving average peak gust wind speed to the associated 10-minute mean wind speed.

The velocity gust factor G_u or the ratio of the gust wind velocity to the mean wind velocity at the reference mid-roof height is defined in terms of g_u and I_u as shown in Eq. (7).

$$G_u = \frac{V_h}{\bar{V}_h} = 1 + g_u I_u \quad (7)$$

Using Eq. (7) with measured values for I_u of 0.23 and $g_u = 3.4$ results in a value of $G_u = 1.78$. Shape factors can be calculated in a form consistent with AS/NZS 1170.2:2011 as $C_{fig} = C_{peak} / G_u^2$.

3. Results and analysis

The results were analyzed to determine effective aerodynamic shape factors. In order to consolidate the results from this analysis, critical values (maximum or minimum) from each of the twenty-four different wind directions were grouped into four main orthogonal directions, namely; $0^\circ \pm 45^\circ$, $90^\circ \pm 30^\circ$, $180^\circ \pm 45^\circ$ and $270^\circ \pm 30^\circ$.

Fig. 6 shows the (minimum) aerodynamic shape factors for the baseline building with a roof pitch of 22.5° and the wind approach direction of $270 \pm 30^\circ$. The peak suction pressures applied in the separation region at the windward gable end on this leading edge of the roof were shown to be satisfactorily represented by the C_{fig} values in AS/NZS1170.2:2011, by Ginger *et al.* (2011). However, the peak suction pressures measured for the baseline building for wind parallel to the ridge (i.e. $270 \pm 30^\circ$) to the middle portion of the roof and the peak positive (i.e., acting towards the surface) pressures at the gable end were found to be larger than those specified in AS/NZS1170.2:2011. This is because AS/NZS 1170.2 is not always conservative, in certain local regions.

The external pressure coefficients on the roof of the 7.5° , 15° and 22.5° baseline building roof and the roof with the array of panels installed on six different parts of the roof and the top, bottom and net panel pressures were measured and analysed in the report by Ginger *et al.* (2011). The characteristics of the pressures on the panels and the effect of the panels on the pressures to the building roof below the panels were similar across the range of roof slopes. The results from this report were used to produce design data for solar panel arrays given in AS/NZS1170.2.

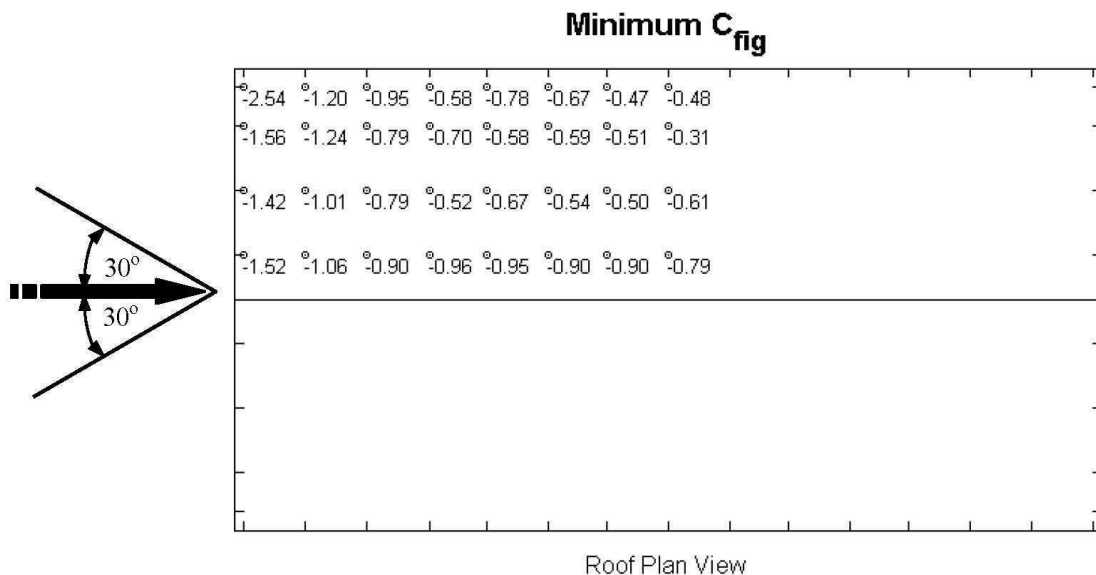


Fig. 6 Minimum aerodynamic shape factors for “Baseline Building - Roof Pitch 22.5° , Wind Direction $270^\circ \pm 30^\circ$ ”

3.1 Detailed analysis for array at position B and D on 22.5° pitched roof

This section describes analyses of the results for the 22.5° slope roof with the solar array at Positions D and B (i.e., near the gable and the central part of the roof). Fig. 7 shows the solar array in these two alternative locations, the labelling of the seven panels, the schematic layout of the pressure taps on the top and bottom surfaces of the panels and the roof, as well as the angles for the approach wind directions.

3.1.1 Pressure coefficients on panel and roof

The mean and peak (minimum and maximum) pressure coefficients obtained on the roof with the solar array fitted with a gap of 100 mm, to Position D for wind blowing from the 270° direction are shown using the three *Roof Plan Views* given as part of Fig. 8. The high suction pressures applied in the separation region at the windward gable end for parts of the roof not under the array can be seen on the plan for minimum C_p .

The mean and minimum C_p values for the top of the roof *underneath the panel array* have significantly smaller magnitudes than for the adjacent parts of the roof not under the panels. In contrast, the maximum roof pressure underneath the first windward half of the panel array is significantly larger than the adjacent parts of the roof without panels. The confined flow between the panels and the roof surface disrupts the formation of vortices and flow separation thus reducing the suction pressures and producing an increase in the positive pressure.

Fig. 8 also includes nine *Panel Plan Views* to document the peak and mean panel pressure coefficients for the top surface, bottom surface and net (i.e., top – bottom) of the panels. The mean C_{ps} to the top of the panel have similar values to the mean C_p values for top roof surface on either side of the panels. The minimum C_{ps} to the bottom of the panels also have very similar values to the corresponding minimum C_{ps} to the top of the roof under the panels. The mean net pressure coefficients, C_{pn} , to the panels can be seen to decrease (that is become less negative) from a value of about -1.5 at the leading Panel 1 to essentially zero for Panel 7.

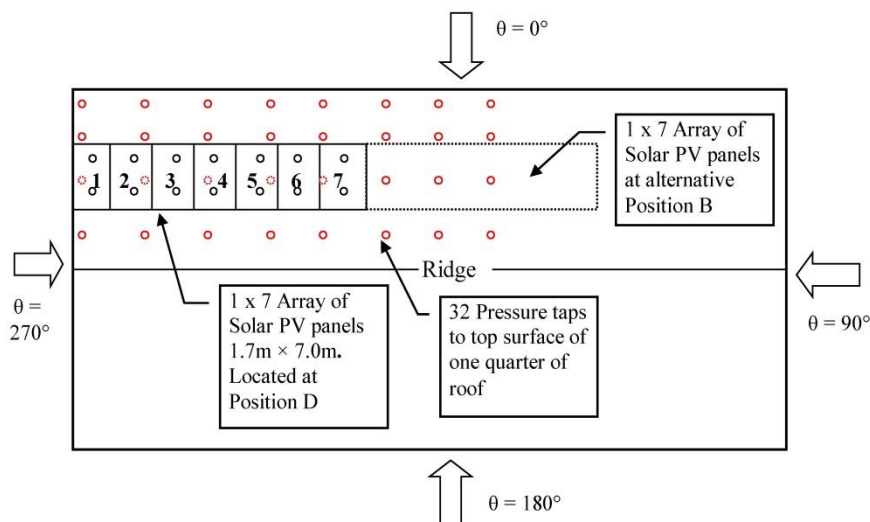


Fig. 7 Locations of solar panel array at Positions B and D on the roof of house

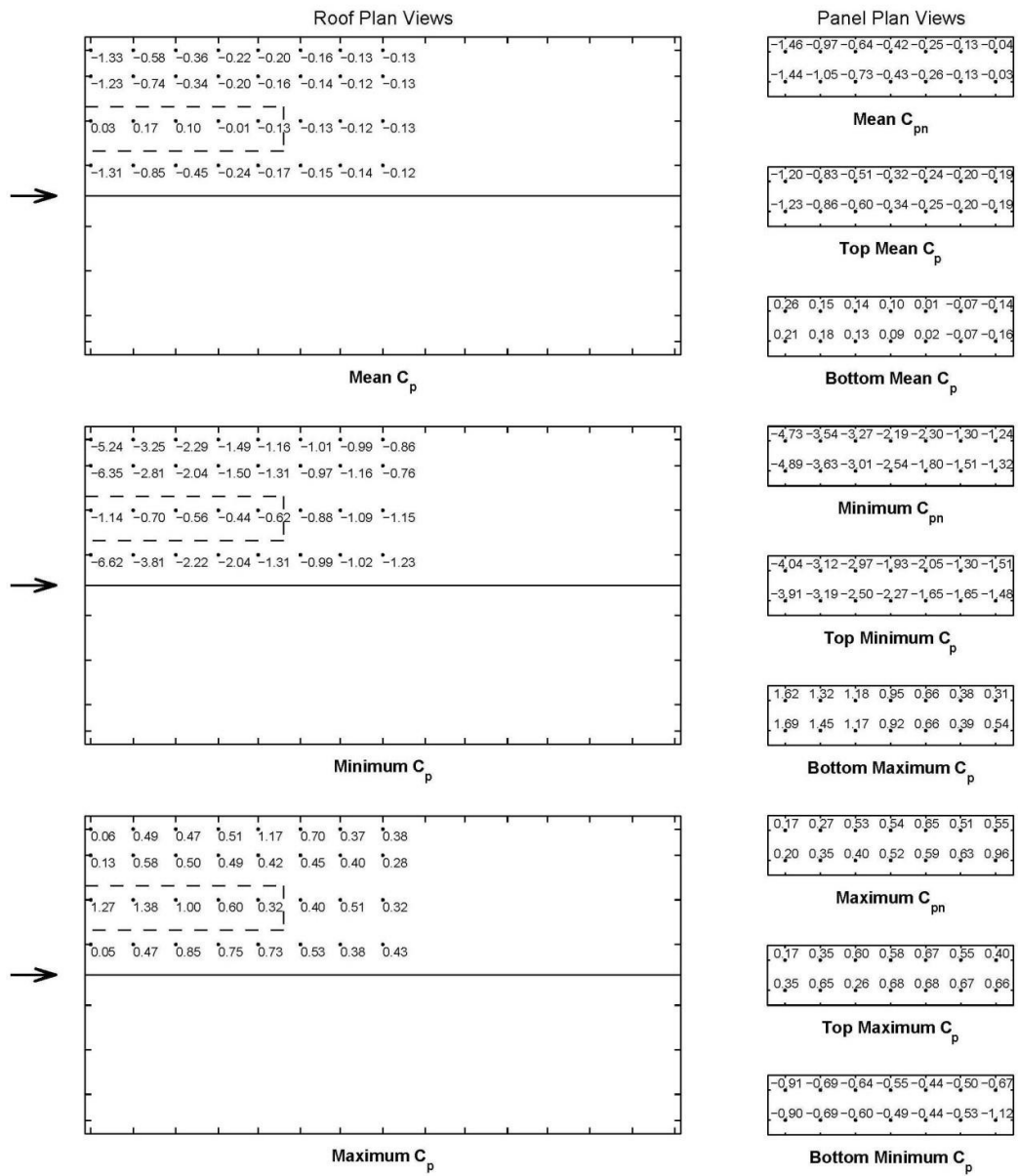


Fig. 8 Mean and Peak C_p s and C_{pn} s for Array Position D, Gap 100 mm – Roof Pitch 22.5°, Wind Direction 270°

Fig. 9 documents the same parameters as shown in Fig. 8, but with the gap of 200 mm below the panels and shows that this larger gap does not have a significant effect on the wind loads on the panels or the roof, as detailed by Ginger *et al.* (2011).

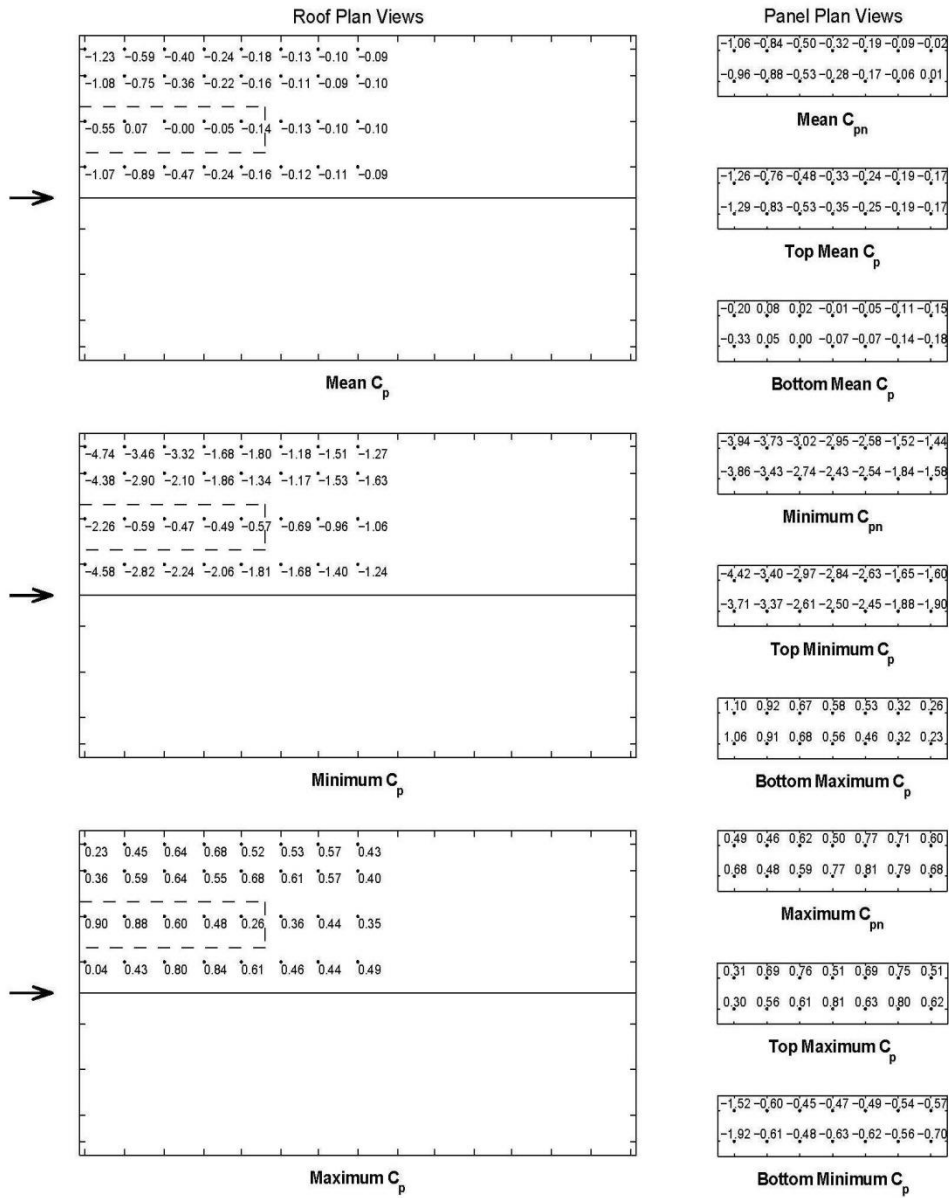


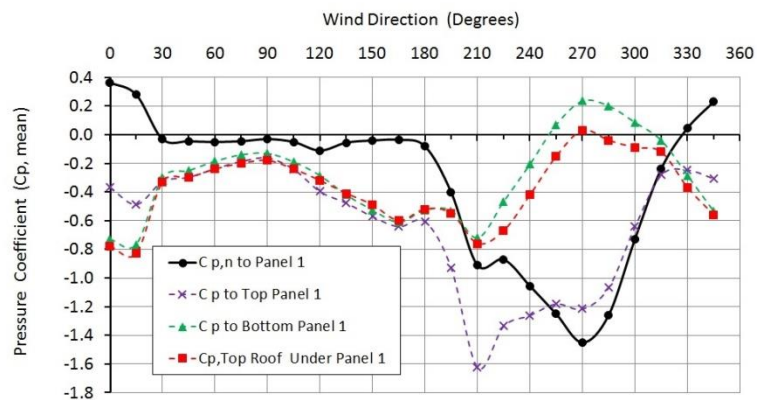
Fig. 9 Mean and Peak C_p s and C_{pn} s for Array Position D, Gap 200 mm – Roof Pitch 22.5°, Wind Direction 270°

Figs. 10(a)-10(d) show the variations of mean pressure coefficients with wind directions (0° to 345°) for Panels 1, 2, 4 and 7, respectively for the 22.5° roof slope building for the 1 × 7 panel array located at Position D with a gap of 100 mm between top of the roof and the underside of the panel. The four parameters plotted are the mean net pressure coefficient values for each

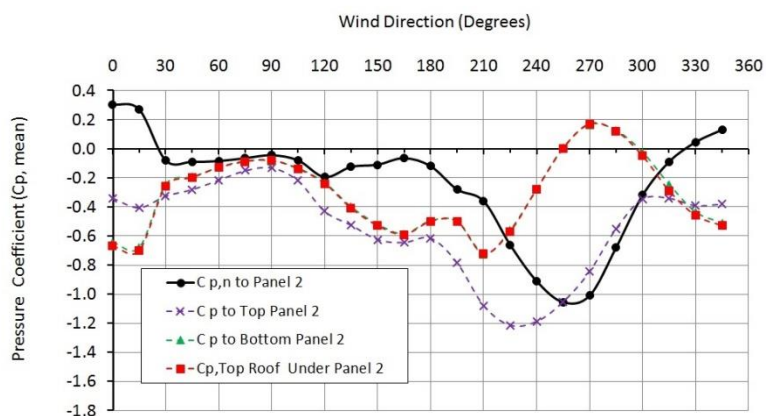
Panel ($C_{p,n}$), mean pressure coefficients for the top and bottom of each Panel ($C_{p,top}$ & $C_{p,bot}$) and the mean pressure coefficient for the top of the roof under each Panel ($C_{p,roof}$).

Figs. 10(a)-10(d) show that for any given wind direction, the net mean pressure on each panel is obtained by subtracting mean pressure on the bottom of the panel from the mean pressure coefficient on the top of the panel. These plots also show that the mean pressure coefficients for the bottom of the panel are similar to those for the roof under the panel for most wind directions. This is similar to the results obtained by Stenabaugh *et al.* (2011) for a similar gap between the underside of the panel and the roof.

Fig. 10(a) shows that the largest net uplift (negative) mean pressure coefficient on Panel 1 occurs for a wind direction of 270° , when this panel is located at the leading gable edge of the roof, with the wind blowing parallel to the ridge. However, the mean uplift pressure coefficient for the top of Panel 1 is about 10% larger than the net mean value across the panel and occurs for a wind direction of 210° .

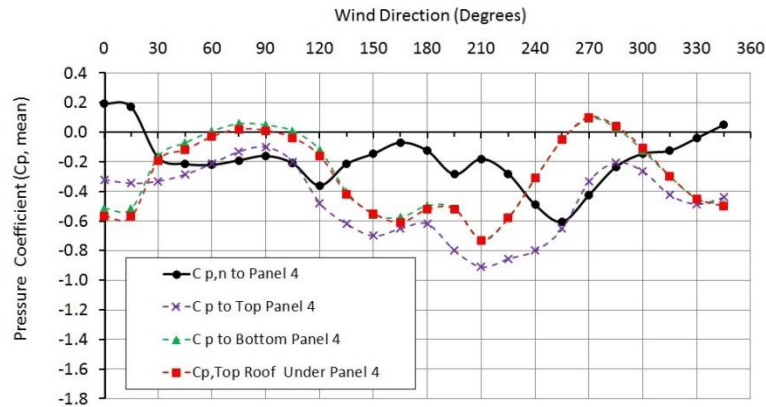


(a)

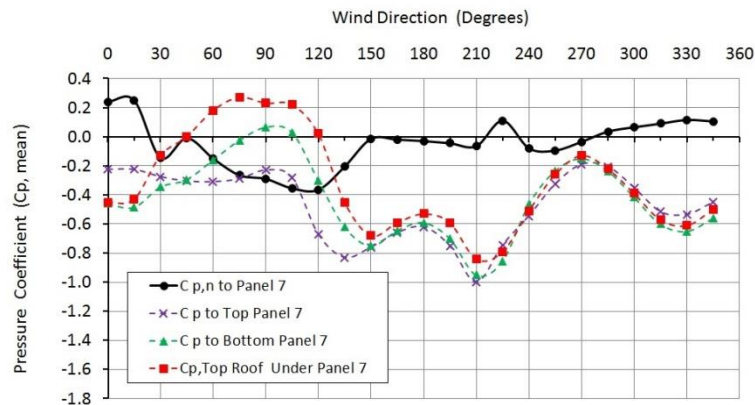


(b)

Continued-



(c)



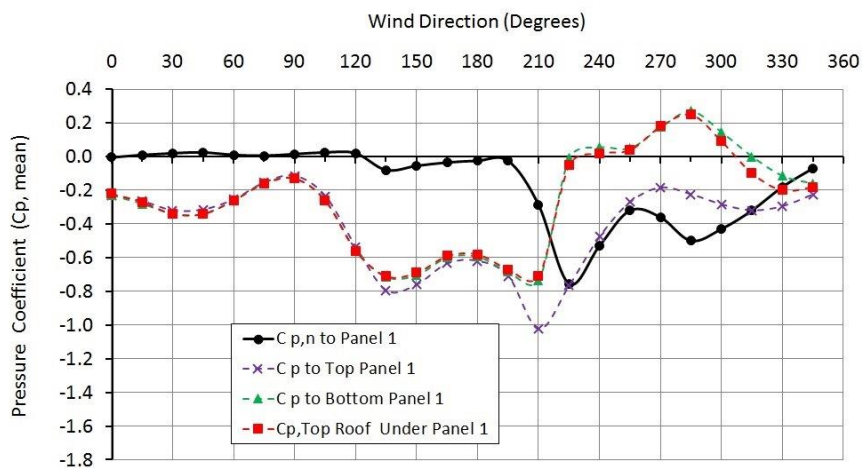
(d)

Fig. 10 (a) Mean Pressure Coefficients for Panel 1 Array Located at Position D, Gap 100mm - Roof Pitch 22.5°, (b) Mean Pressure Coefficients for Panel 2 Array Located at Position D, Gap 100 mm - Roof Pitch 22.5°, (c) Mean Pressure Coefficients for Panel 4 Array Located at Position D, Gap 100mm - Roof Pitch 22.5° and Mean Pressure Coefficients for Panel 7 Array Located at Position D, Gap 100mm - Roof Pitch 22.5°

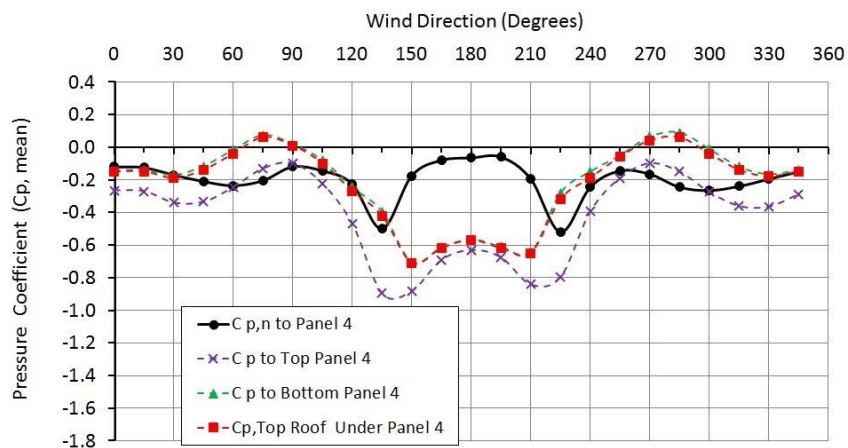
Fig. 10(b) for Panel 2, shows the same trends as observed for Panel 1, but with slightly smaller values. Here the largest net mean uplift value for this panel (which is the second panel in from the gable end) occurs for a wind direction of 255°, effectively when the wind is blowing parallel to the ridge. This largest negative value (-1.06) is significantly less than the highest value for Panel 1 (-1.45 for wind direction 270°). Again the mean uplift pressure coefficient to the top of Panel 2 is about 10% larger than the net mean value across the panel, and occurs for a wind direction of 225°.

Fig. 10(c) for Panel 4 (the central panel in the array), shows that the net uplift loads are in general smaller in magnitude than on Panel 1 and Panel 2. Fig. 10(d) for Panel 7 shows that there is a further reduction in the net uplift loads except for wind directions between 60° and 120°. This effect occurs because Panel 7 becomes effectively a “leading edge panel” for these wind directions.

Figs. 11(a) and 11(b) show the same four mean pressure coefficients for Panel 1 and Panel 4 respectively, for the array located at Position B, effectively the middle third of the roof. Again, the mean pressure coefficients for the bottom of the panel are virtually identical to those for the roof under the panel for all wind directions. Fig. 11(a) shows that the largest net mean uplift of (-0.8) occurs for a wind direction of 225°. Even though Panel 1 is on the leeward side of the roof for this wind direction, it is still the “Leading” panel of the array. Fig. 11(b) shows that the largest net mean uplift of about (-0.55) is applied to Panel 4 for a wind direction of 225°. It can also be seen that all four plots in Fig. 11(b) are mirror images about an axis about the 180° wind direction.



(a)



(b)

Fig. 11 Mean Pressure Coefficients for Panel 1 Array Located at Position B, Gap 100 mm - Roof Pitch 22.5° and (b) Mean Pressure Coefficients for Panel 4 Array Located at Position B, Gap 100 mm - Roof Pitch 22.5°

3.2 Aerodynamic shape factors

This section presents aerodynamic shape factors in a form compatible with AS/NZS1170.2:2011 on the array located at Positions B or D (and the roof under the Panels) for wind blowing from the $270 \pm 30^\circ$ sector, and the $0 \pm 45^\circ$ sector.

Fig. 12 shows a schematic part roof plan of the model for the case of wind blowing parallel to the ridge (wind direction $270 \pm 30^\circ$) with the solar array located at either Position B or Position D. Also shown in this figure is a schematic section (Section A – A), taken with its cutting plane parallel to the ridge and passing through the nominal mid width of the solar panels. Five different aerodynamic shape factors at locations along this section plane through the roof, as listed, are presented:

1. ($C_{fig, rf, no\ pan}$) –minimum aerodynamic shape factor for the top of the roof surface without any panels fitted (baseline building).
2. ($C_{fig, rf\ under\ pan}$) –minimum aerodynamic shape factor for the top of the roof surface directly under the panels.
3. ($C_{fig, n}$) –minimum net aerodynamic shape factor for the panels.
4. ($C_{fig, bot\ pan}$) –minimum aerodynamic shape factor for the bottom surface of the panels.
5. ($C_{fig, top\ pan}$) –minimum aerodynamic shape factor for the top surface of the panels.

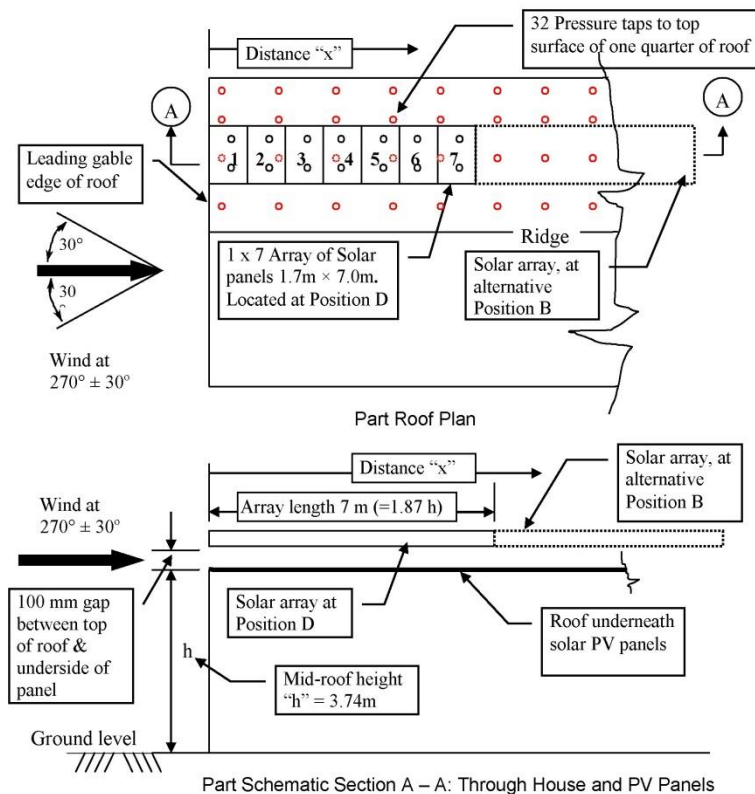


Fig. 12 Part plan and part schematic section of house model with array of solar PV panels fitted to Position D or alternative Position B (Dimensions noted are equivalent full-scale)

Fig. 13(a) provides plots of these minimum aerodynamic shape factors (minimum being defined as the largest negative values, causing loads acting away from the surface) versus the non-dimensional relative distance (x/h) along the roof, when the array is located at Position D. Aerodynamic shape factors for the roof without panels, as specified in AS/NZS1170.2:2011 are also plotted and are seen to be in good agreement with the calculated aerodynamic shape factors for the “baseline” building without solar panels, up to a relative distance (x/h) of about 2. However, for (x/h) values larger than 2, the measured values for the aerodynamic shape factor to the baseline building are larger than the code values, because AS/NZS1170.2:2011 is not always conservative in certain local regions.

The plots in this figure show several distinct trends. Firstly, the minimum net aerodynamic shape factors on the panels decrease from the largest negative value of -1.48 on Panel 1 (immediately adjacent to the leading gable end) to the smallest negative value of -0.46 to Panel 7. Secondly, these minimum net aerodynamic shape factors are similar to both the minimum aerodynamic shape factors to the top of the roof without panels ($C_{\text{fig, rf, no pan}}$) and the top of the panels ($C_{\text{fig, top pan}}$) with the largest values at the leading edges of the roof and panels. This essentially means that the introduction of a panel array does not impose any additional loads on the “overall system in this part of the roof”.

The minimum aerodynamic shape factors for the bottom of the panels ($C_{\text{fig, bot pan}}$) and the top of the roof under the panels ($C_{\text{fig, rf under pan}}$) have very similar values. It can also be seen that these minimum negative (away from the surface) values are significantly smaller than those on the roof when panels are not fitted.

Similar plots, for the maximum (towards the surfaces) aerodynamic shape factors are provided in Fig. 13(b). This figure shows that the values for the maximum net aerodynamic shape factors on the panels increase from a value of 0.19 on Panel 1 (immediately adjacent to the leading gable end) to the largest positive value of 0.38 to Panel 7. The maximum pressure for the top of the roof under the panels and the underside of the panels are almost identical, this indicates a consistent pressure to the underside of the panels and the immediately adjacent top roof surface within the void beneath the panels and is the same pattern as observed for the minimum values.

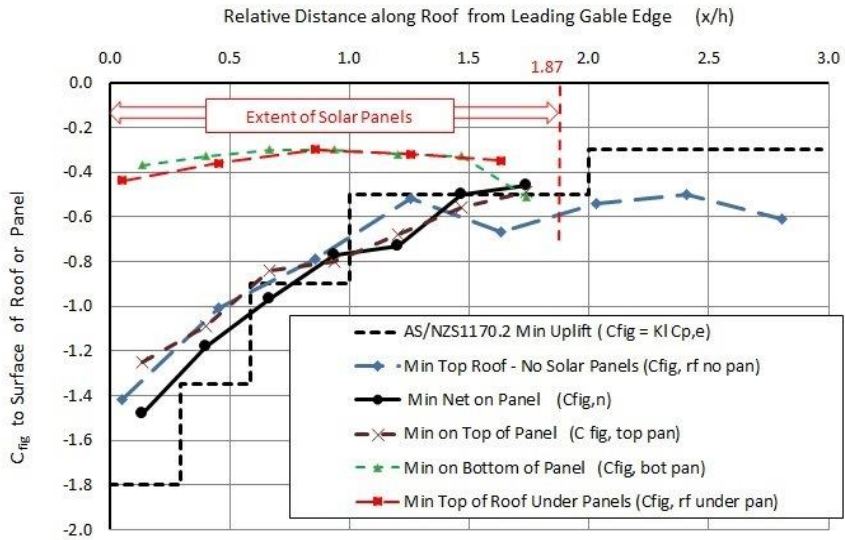
In summary, the net negative aerodynamic shape factors on the panels ($C_{\text{fig, n}}$), producing forces acting upwards, range from about (-1.5) at the leading edge to about (-0.6), and the net positive aerodynamic shape factor is about (+0.4) for with wind blowing from the $270 \pm 30^\circ$ sector.

Fig. 14(a) provides plots of the same five minimum aerodynamic shape factors but for the panel array located at Position B. There is a trend of decreasing values for the minimum net aerodynamic shape factors on the panels, from the most windward (Panel 1 with the largest negative value of -0.87) to the most leeward (Panel 7 with the smallest negative value of -0.23). However, the net minimum aerodynamic shape factors for the windward part of the array (i.e., Panels 1 to 3) have significantly larger values than corresponding values for the roof without any panels fitted. This means that when panels are fitted to this part of the roof, the roof structure under these panels may be subjected to larger loads than for the case of no panels fitted.

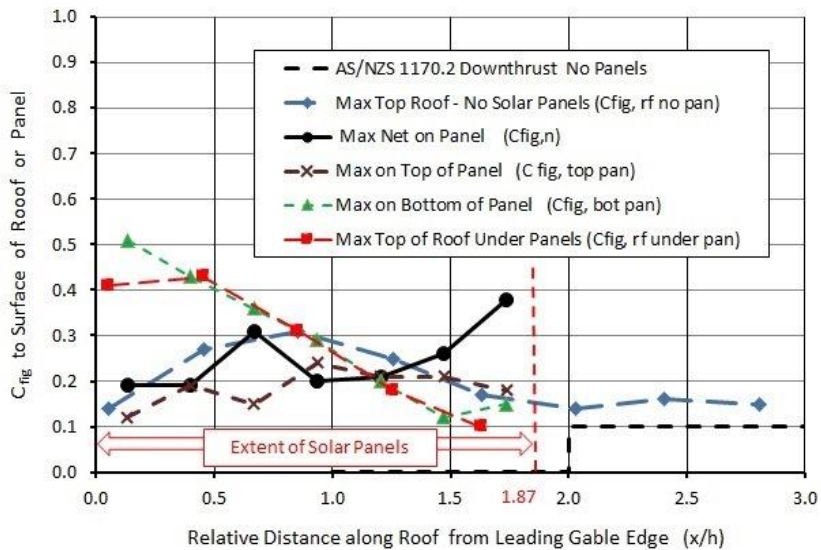
Again, the minimum aerodynamic shape factors for the bottom of the panels ($C_{\text{fig, bot pan}}$) and the top of the roof under the panels ($C_{\text{fig, rf under pan}}$) have very similar values, and are significantly greater than the values provided in the Australian Standard.

Fig. 14(b) provides plots for the maximum (towards surface) aerodynamic shape factors for the array located at Position B, and again the maximum aerodynamic shape factors for the bottom of the panels ($C_{\text{fig, bot pan}}$) and the top of the roof under the panels ($C_{\text{fig, rf under pan}}$) have very similar values.

The largest magnitude net aerodynamic shape factors on the panels ($C_{fig,n}$), for this array in the central one third of the roof, is about (-0.9) in the uplift (minimum) direction and is about (+0.3) in the downwards (maximum) direction.

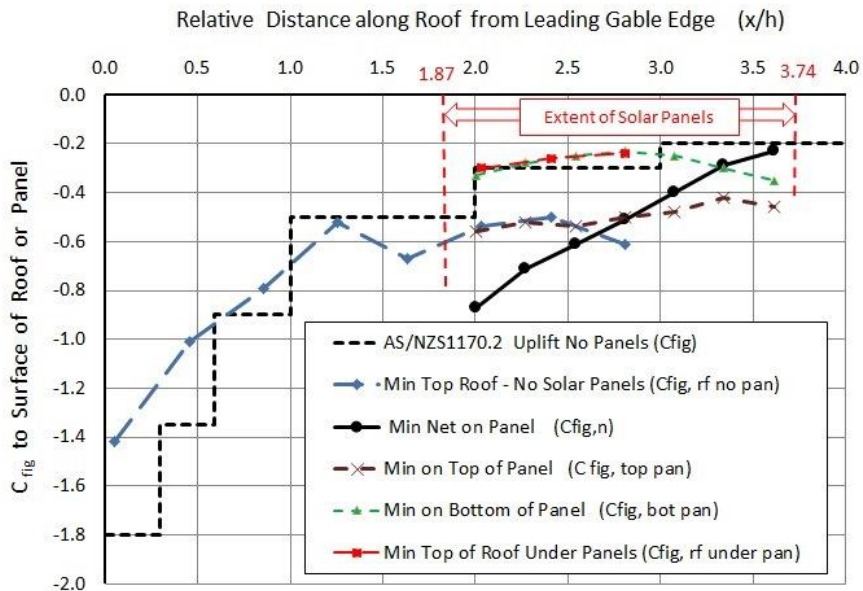


(a)

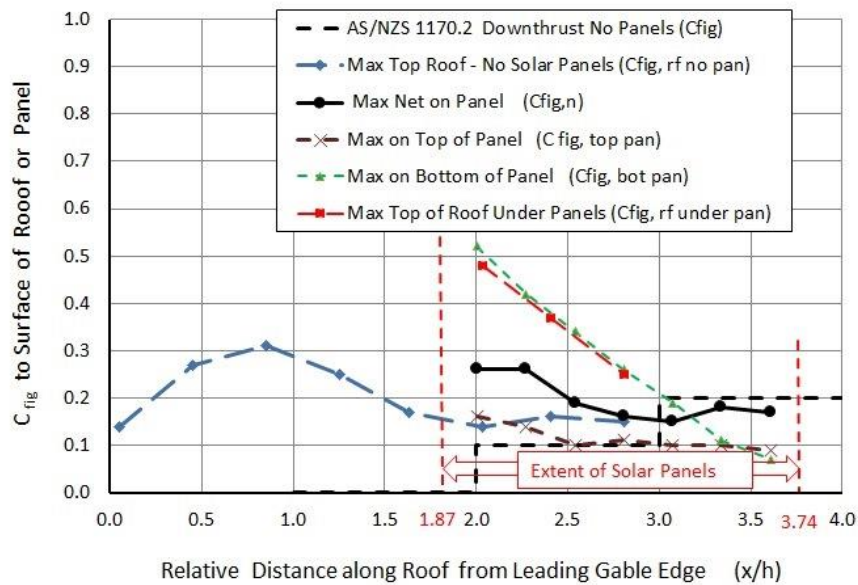


(b)

Fig. 13 (a) Minimum C_{fig} –Array Position D, Gap 100 mm - Roof Pitch 22.5°, Wind Direction 270° ± 30° and (b) Maximum C_{fig} –Array Position D, Gap 100 mm - Roof Pitch 22.5°, Wind Direction 270° ± 30°



(a)



(b)

Fig. 14 (a) Minimum C_{fig} –Array Position B, Gap 100 mm - Roof Pitch 22.5° , Wind Direction $270^\circ \pm 30^\circ$ and (b) Maximum C_{fig} –Array Position B, Gap 100 mm - Roof Pitch 22.5° , Wind Direction $270^\circ \pm 30^\circ$

Table 1 Aerodynamic Shape Factor ($C_{fig,n}$) for panels in arrays at Position D and Position B, Gap 100 mm - Roof Pitch 22.5°, for Wind Direction $0^\circ \pm 45^\circ$ and $270^\circ \pm 30^\circ$ (Values from Ginger *et al.* (2011))

Panel No.	$C_{fig,n}$ for Panels							
	Wind Direction $0^\circ \pm 45^\circ$				Wind Direction $270^\circ \pm 30^\circ$			
	Array at Position D (Upwind End)		Array at Position B (Upwind Central)		Array at Position D (Upwind End)		Array at Position B (Upwind Central)	
	Min	Max	Min	Max	Min	Max	Min	Max
1	-0.86	0.55	-0.56	0.26	-1.48	0.19	-0.87	0.26
2	-0.50	0.49	-0.43	0.28	-1.18	0.19	-0.71	0.26
3	-0.42	0.40	-0.43	0.23	-0.97	0.31	-0.61	0.19
4	-0.44	0.41	-0.37	0.23	-0.77	0.20	-0.51	0.16
5	-0.52	0.39	-0.39	0.23	-0.73	0.21	-0.40	0.15
6	-0.62	0.37	-0.46	0.26	-0.50	0.26	-0.29	0.18
7	-0.60	0.43	-0.77	0.30	-0.46	0.38	-0.23	0.17

The net aerodynamic shape factors for the Panels (1 to 7) when the arrays are located at either Position D or Position B with a gap of 100 mm, roof slope of 22.5° and wind blowing from the $0^\circ \pm 45^\circ$ and $270^\circ \pm 30^\circ$ sectors are summarized in Table 1.

Examining Fig. 13(a) through to Fig. 14(b) it can be seen that a slightly conservative encompassing value for the aerodynamic shape factors applying to the top of the roof surface under panels when the wind is blowing parallel to the ridge ($\theta = 270^\circ$) can be specified as $C_{fig, rf \text{ under pan}} = \pm 0.5$. Based on this data (and the larger data set presented by Ginger *et al.* 2011), the aerodynamic shape factors for the top of the roof surface under panels when the wind is blowing perpendicular to the ridge ($\theta = 0^\circ \pm 45^\circ$) can be specified as $C_{fig, rf \text{ under pan}} = \pm 0.6$.

3.3 Recommended aerodynamic shape factors for codification

Results from Ginger *et al.* (2011) were used to produce net aerodynamic shape factors on solar panels mounted parallel to a roof surface with a gap of between 50 mm to 300 mm above the roof, with a roof slope (α) of between 5° and 30°, in AS/NZS 1170.2:2011. Table 2 reproduces part of Table D11 from that standard that provides the uplift and down-acting net aerodynamic shape factors on solar panels. However, AS/NZS 1170.2:2011 does not specifically provide aerodynamic shape factors for the top of a roof beneath solar panels.

Based on the analysis reported in this paper, the following values are suggested for the aerodynamic shape factors for the top of the roof surface under the panels:

$C_{fig, rf \text{ under pan}} = \pm 0.5$ when the wind is blowing parallel to the ridge ($\theta = 270^\circ$) and

$C_{fig, rf \text{ under pan}} = \pm 0.6$ when the wind is blowing perpendicular to the ridge ($\theta = 0^\circ$)

Table 2 Aerodynamic Shape Factor ($C_{fig,n}$) for different array positions and roof slopes for Wind Perpendicular to the ridge ($\theta = 0^\circ$) and Parallel to the ridge ($\theta = 270^\circ$) Directions (Part copy of Table D11 from AS/NZS1170.2 (2011))

Description of Array Position (See also Fig D9 in AS/NZS1170.2)	$(C_{fig,n})$ Values for Different Wind Directions, Array Positions & Roof Slopes			
	$(\theta = 0^\circ)$ and $20^\circ \leq \alpha \leq 30^\circ$		$(\theta = 270^\circ)$ and $5^\circ \leq \alpha \leq 30^\circ$	
	Uplift	Down	Uplift	Down
Upwind End	-1.0	+0.6		
Upwind Central	-0.8	+0.3		
Upwind End (Upwind one third of roof)			-1.7	+0.4
Central (Central one third of roof)			-1.2	+0.5
Downwind End (Downwind one third of roof)			-1.1	+0.5

4. Conclusions

The results and analysis for this study that considered the wind loads acting on solar panels attached parallel to sloped roofs, and acting on the underlying roof, showed that:

- The panel closest to the leading gable edge of the roof is subjected to the largest net upwards-acting pressures.
- For wind blowing parallel to the ridge, the net negative pressures on the panels ($C_{fig,n}$) attached near the gable end (Position D), are very similar to the external pressures for the roof without panels fitted ($C_{fig, rf, no pan}$).
- The variation in size of the gap between the array and the roof did not have a significant effect.
- Because the gap under the panels and between the rails is so narrow, it acts in a similar manner to a conduit, with both the maximum (acting into the surface) and minimum (suction) pressures being very similar for both the top of the roof and the underside (bottom) of the panels.

For solar arrays in the middle portion of the roof (Position B), the net load to the arrays is larger than that on the roof without any solar panels. This means that the supporting roof structure will be subjected to larger upwards-acting and downwards-acting loads, after solar panels are fitted to these parts of the roof.

Aerodynamic shape factors for the top of the roof surface located under solar panels have been determined, and values of $C_{fig, rf under pan} = \pm 0.5$ when the wind is blowing parallel to the ridge ($\theta = 270^\circ$) and $C_{fig, rf under pan} = \pm 0.6$ when the wind is blowing perpendicular to the ridge ($\theta = 0^\circ$) are suggested for consideration for inclusion in AS/NZS 1170.2:2011.

Acknowledgements

The authors acknowledge the significant contribution by Mr. Matt Payne to the experimental and analysis work performed for the wind tunnel study as part of his final year undergraduate thesis project.

References

- American Society of Civil Engineers (2010). ASCE **7-10**, *Minimum design loads for buildings and other structures*, ASCE Reston, Virginia, USA.
- Australasian Wind Engineering Society (AWES). (2001), *Quality Assurance Manual for Wind-Engineering Studies of Buildings* (AWES-QAM-1).
- Cao, J., Tamura, Y. and Yoshida, A. (2013), "Wind tunnel investigation of wind loads on rooftop modules for green roofing systems", *J. Wind Eng. Ind. Aerod.*, **118**, 20-34.
- Ginger, J., Payne, M., Stark, G., Sumant, B. and Leitch, C. (2011), *Investigation of wind loads applied to solar panels mounted on roofs*. James Cook University, Cyclone Testing Station, Technical Report No. TS821. PDF copy of report at: <https://www.jcu.edu.au/cts/publications/content/technical-reports/investigation-on-wind-loads-applied-to-solar-panels-mounted-on-roofs/view>
- Holmes, J.D. and Ginger, J.D. (2012), "The gust wind speed duration in AS/NZS 1170.2", *Australian J. Struct. Eng.*, **13**(3), 207-216.
- Holmes, J.D., Allsop, A.C. and Ginger, J.D. (2014), "Gust durations, gust factors and gust response factors in wind codes and standards", *Wind Struct.*, **19**(3), 339-352.
- Kopp, G.A. (2014), "Wind loads on low profile, tilted, solar arrays placed on large, flat, low-rise building roofs", *J. Struct. Eng. - ASCE*, **140**(2), 04013057.
- Kopp, G.A. and Banks D. (2013), "Use of wind tunnel test methods for obtaining design wind loads on roof mounted solar arrays", *J. Struct. Eng. - ASCE*, **139**(2), 284-287.
- Maffei, J., Telleen, K., Ward, W., Kopp, G.A. and Schellenberg, A., (2014), "Wind design practice and recommendations for solar arrays on low-slope roofs", *J. Struct. Eng. - ASCE*, **140**(2), 04013040.
- Schellenberg, A., Maffei, J., Telleen, K. and Ward, R. (2013), "Structural analysis and application of wind loads to solar arrays", *J. Wind Eng. Ind. Aerod.*, **123**, 261-272.
- Standards Australia (2011), *Structural design actions. Part 2: wind actions*, Australian/New Zealand Standard, AS/NZS 1170.2:2011, Standards Australia, Sydney, New South Wales, Australia.
- Stathopoulos, T., Ioannis, Z. and Xypnitou, E. (2014), "Local and overall wind pressure and force coefficients for solar panels", *J. Wind Eng. Ind. Aerod.*, **125**, 195-206.
- Stenabaugh, S.E., Karava, P. and Kopp, G.A. (2011), "Design wind loads for photovoltaic systems on sloped roofs of residential buildings", *Proceedings of the 13th International Conference on Wind Engineering*, Amsterdam, Netherlands, July 10-15.
- Wood, G.S., Denoon, R.O. and Kwok, K.C.S. (2001), "Wind loads on industrial solar panel arrays and supporting roof structure", *Wind Struct.*, **4**(6), 481-494.